

Supporting Information  
for

**Photo-assisted electrochemical CO<sub>2</sub> reduction at boron-doped diamond cathode**

Goki Iwai, Andrea Fiorani,\* Jinglun Du and Yasuaki Einaga\*

Department of Chemistry, Keio University, Yokohama 223-8522, Japan.

## Table of content

	pp.
<b>1. Boron-doped diamond: SEM micrographs and Raman spectrum</b>	<b>3</b>
<b>2. TiO<sub>2</sub> NT: characterisation</b>	<b>4</b>
<b>3. Photoelectrochemical cell assembly</b>	<b>5</b>
<b>4. HPLC and GC calibration lines</b>	<b>6</b>
<b>5. Light source: emission spectra</b>	<b>7</b>
<b>6. OCP measurements</b>	<b>7</b>
<b>7. Potential, current, and faradaic efficiency of FA for configuration 1</b>	<b>8</b>
<b>8. The <math>\eta_{\text{PAE}}</math> for configuration 1</b>	<b>9</b>
<b>9. Faradaic efficiency for configuration 1 (all products)</b>	<b>9</b>
<b>10. Current without electric bias (<math>E_{\text{tot}} = 0 \text{ V}</math>)</b>	<b>10</b>
<b>11. Potential and current for configuration 2</b>	<b>11</b>
<b>12. Faradaic efficiency for configuration 2 (all products)</b>	<b>11</b>
<b>13. Control experiments for products confirmation</b>	<b>12</b>
<b>14. Efficiency comparison with other PEC systems</b>	<b>13</b>
<b>15. Water oxidation potential at pH 14</b>	<b>13</b>
<b>16. References</b>	<b>13</b>

## 1. Boron-doped diamond: SEM micrographs and Raman spectrum

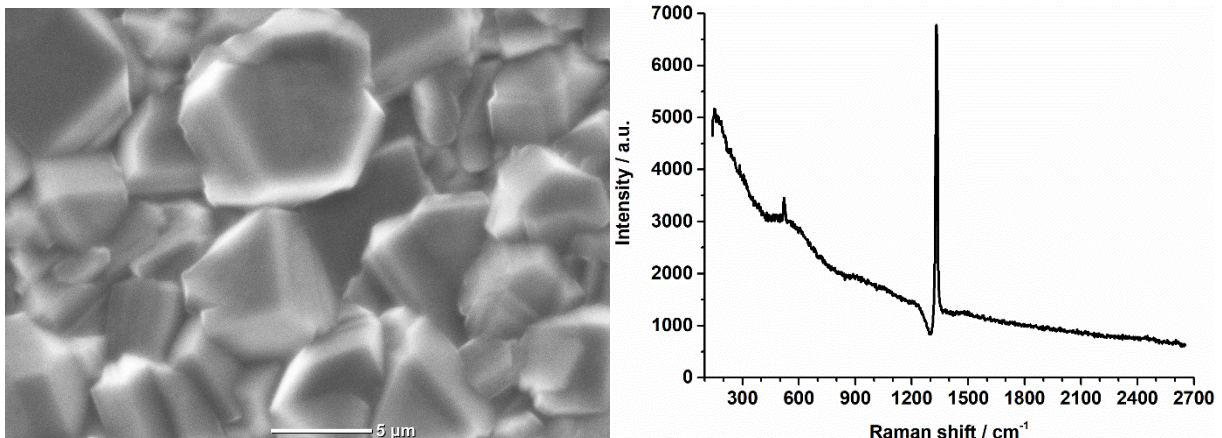


**Fig. S1.** SEM micrograph of BDD showing polycrystalline structure of micrometre size; Raman spectrum showing diamond phonon at  $1332\text{ cm}^{-1}$ , and two weak peaks ( $500$  and  $1200\text{ cm}^{-1}$ ) as result of boron doping (B/C 0.1 %). A peak around  $1530\text{ cm}^{-1}$  (G band) is not evident which indicates the absence of  $\text{sp}^2$  carbon.<sup>1</sup>

## 2. TiO<sub>2</sub> NT: characterisation

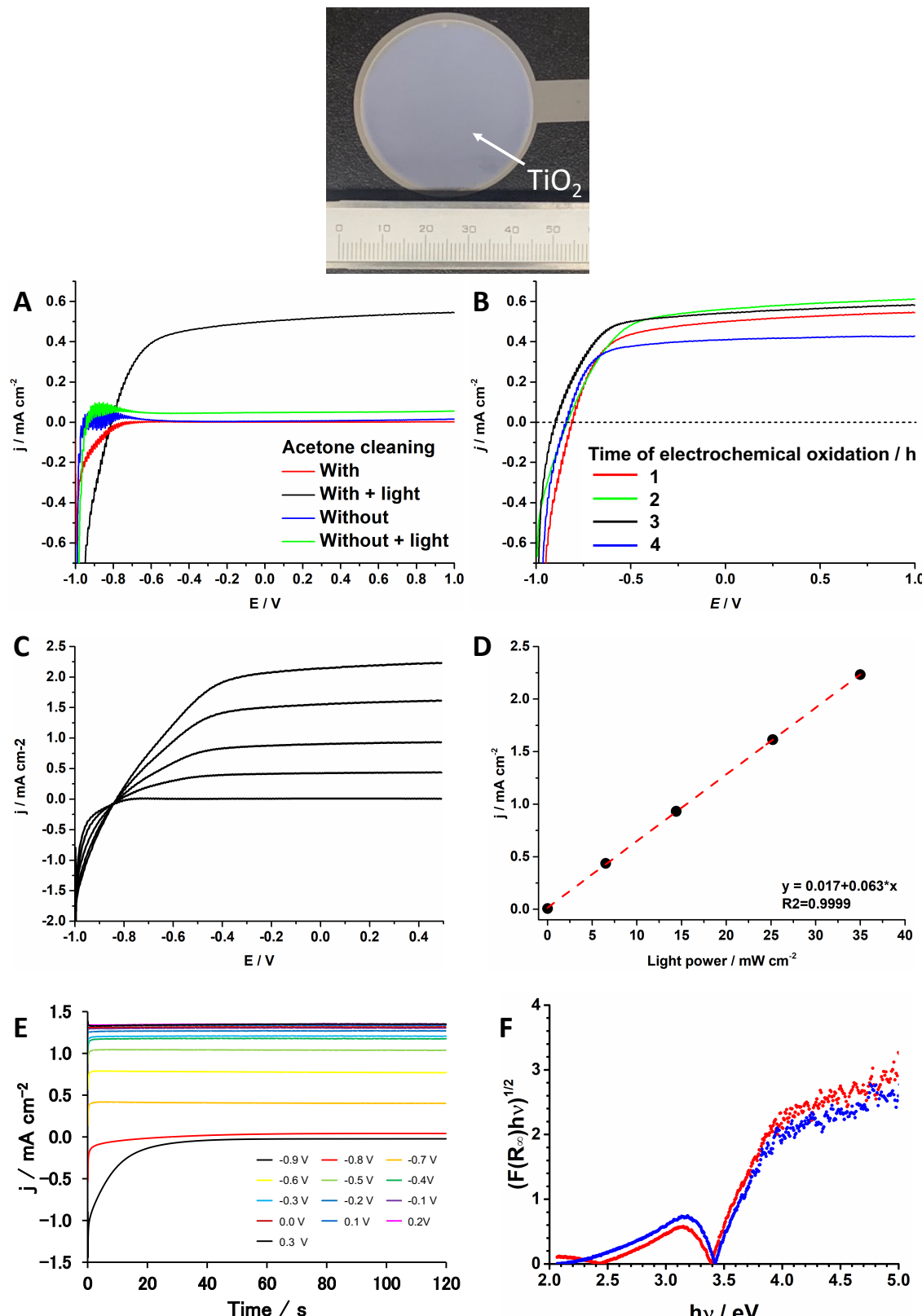


**Fig. S2.** Photograph of the TiO<sub>2</sub> NT electrode; A) Effect of acetone cleaning before electrochemical oxidation; B) Effect of electrochemical oxidation time on photocurrent; C) Response to increase of light power by cyclic voltammetry at 100 mV s<sup>-1</sup>, and D) current as function of light power; E) Chronoamperometry at selected potentials from -0.9 V to 0.3 V; F) Kubelka-Munk plot of two different TiO<sub>2</sub> NT electrodes. Electrolyte: 0.5 M KOH. Light power: 6.5 mW cm<sup>-2</sup> (A and B), 25.2 mW cm<sup>-2</sup> (E). Potential vs Ag/AgCl, KCl (sat'd).

## 2.1. XRD spectrum of Fig.1B.

TiO<sub>2</sub> anatase peaks (PDF 01-070-6826: 25.42°, 38.14°, 38.77°, 48.23°, 54.34°, 55.29° for (101), (004), (112), (200), (105) and (211) planes respectively) are mainly observed. And also, the titanium peaks (PDF 01-089-5009: 35.17°, 38.46° and 53.09° for (100), (002) and (102) planes respectively) are also observed, attributed from the metallic titanium underneath the nanotubes.

## 3. Photoelectrochemical cell assembly

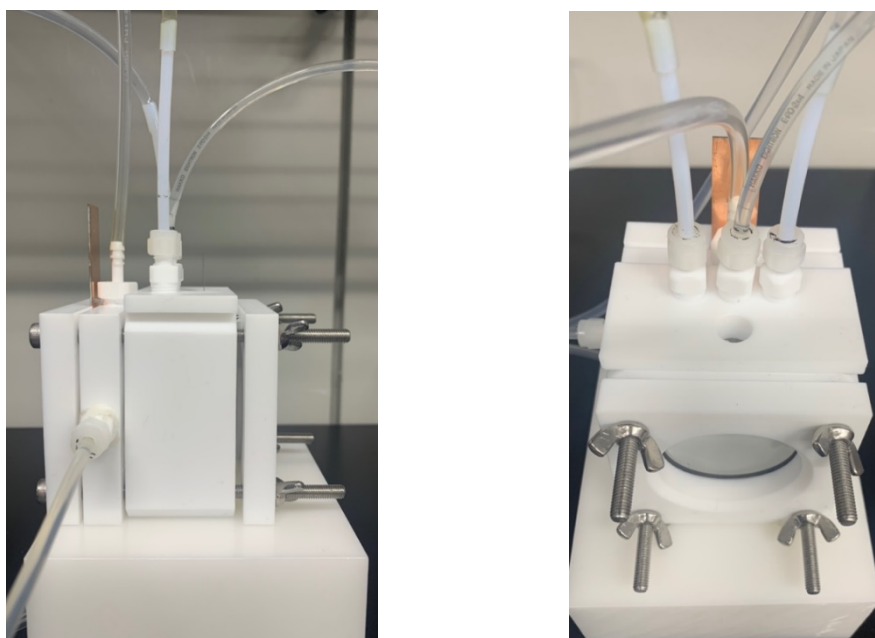


**Fig. S3.** Photograph of photoelectrochemical cell from different directions.

## 4. HPLC and GC calibration lines

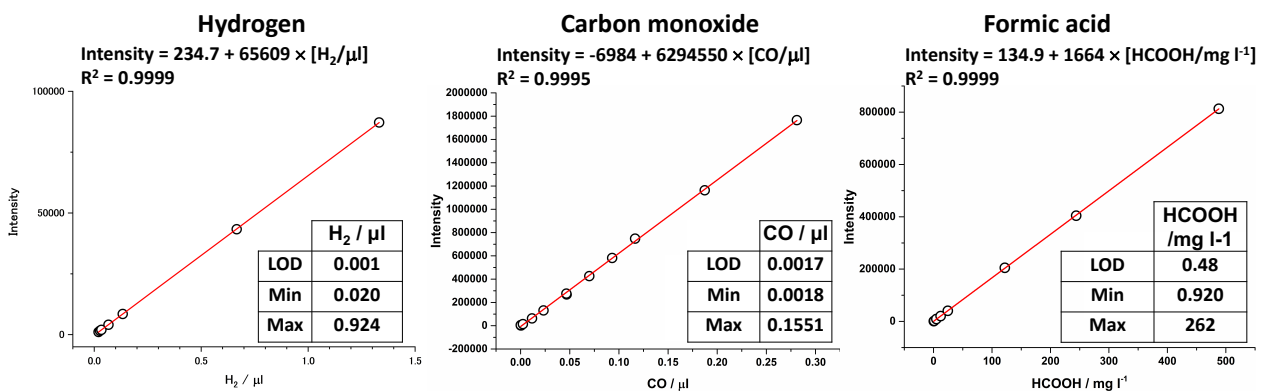


**Fig. S4.** GC and HPLC calibration lines for the quantification of CO<sub>2</sub> reduction products: hydrogen, carbon monoxide, and formic acid. Limit of detection (LOD), minimum and maximum concentrations detected after the CO<sub>2</sub> electrochemical reduction experiments are reported.

## 5. Light source: emission spectra

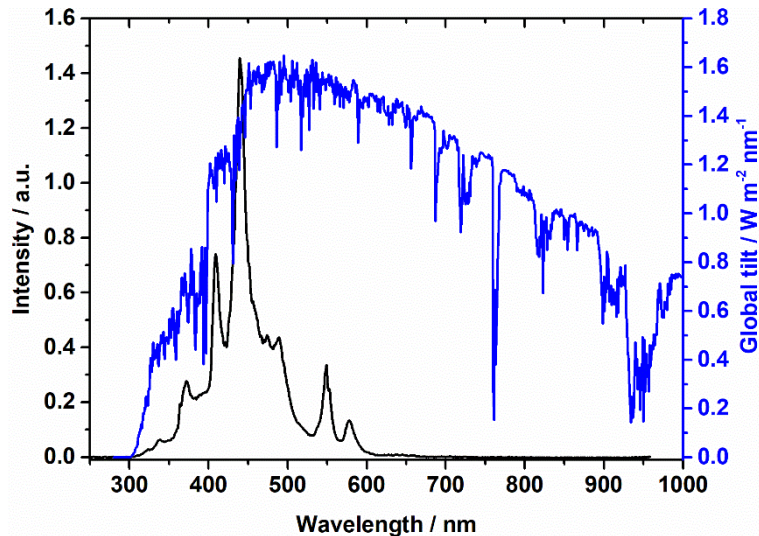


**Fig. S5.** Emission spectrum of light source (black). For comparison purpose only, solar standard radiation: AM1.5 Global tilt spectrum (ASTM G-173-03) from the National Renewable Energy Laboratory (blue) <https://www.nrel.gov/grid/solar-resource/spectra-am1.5.html>. The light source wavelength range is within the solar spectrum.

## 6. OCP measurements

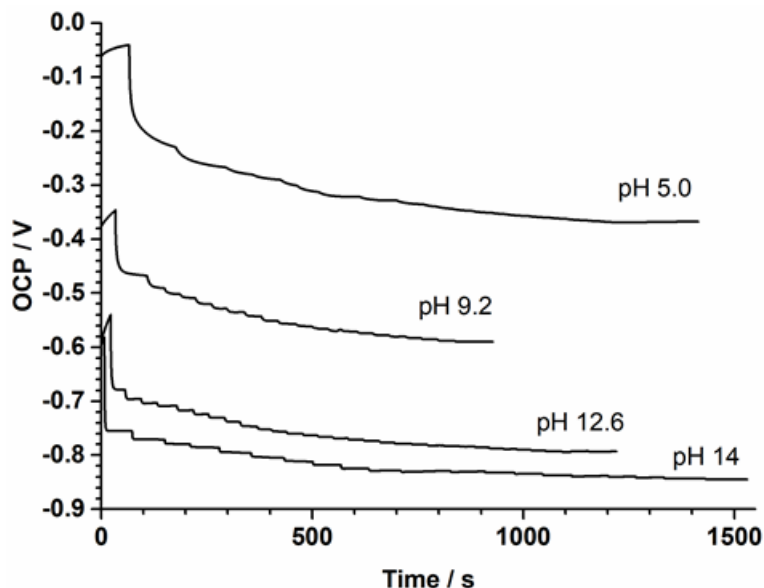


**Fig. S6.** OCP measurement at different pH: 5.0, 9.2, and 12.6 in 0.1 M phosphate buffer, and 14 in 0.5 M KOH. Light power was increased gradually from 0.7 to 14.4  $\text{mW cm}^{-2}$ . Potential vs Ag/AgCl, KCl (sat'd).

## 7. Potential, current, and faradaic efficiency of formic acid for configuration 1

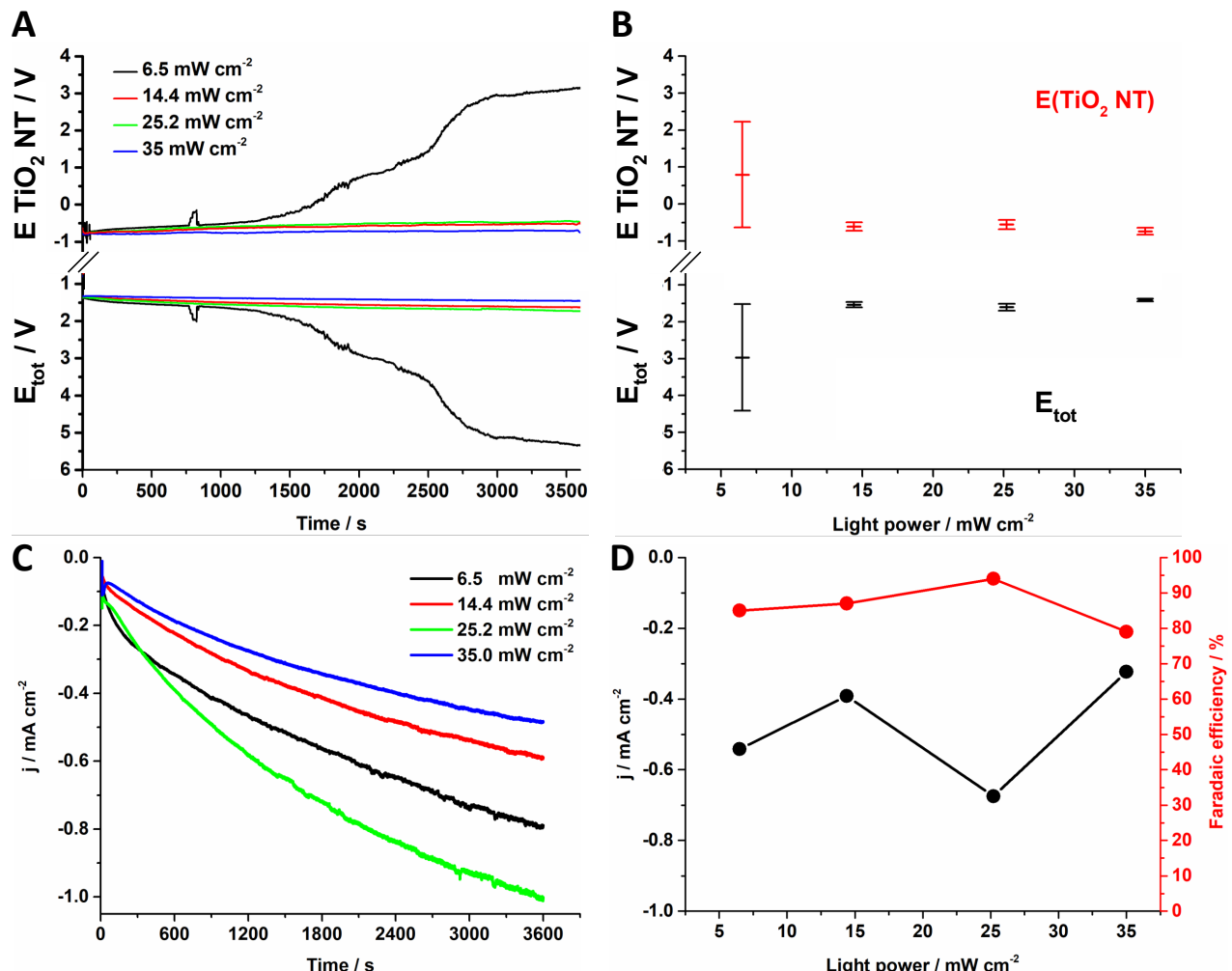


**Fig. S7.** A) Potential monitoring:  $E(\text{TiO}_2 \text{ NT})$  and  $E_{\text{tot}}$ ; B) average potential and variation (standard deviation); C) current density; D) average current density and faradaic efficiency for formic acid production. The potential  $E \text{ TiO}_2 \text{ NT}$  is vs Ag/AgCl, KCl (sat'd).

## 8. The $\eta_{PAE}$ for configuration 1

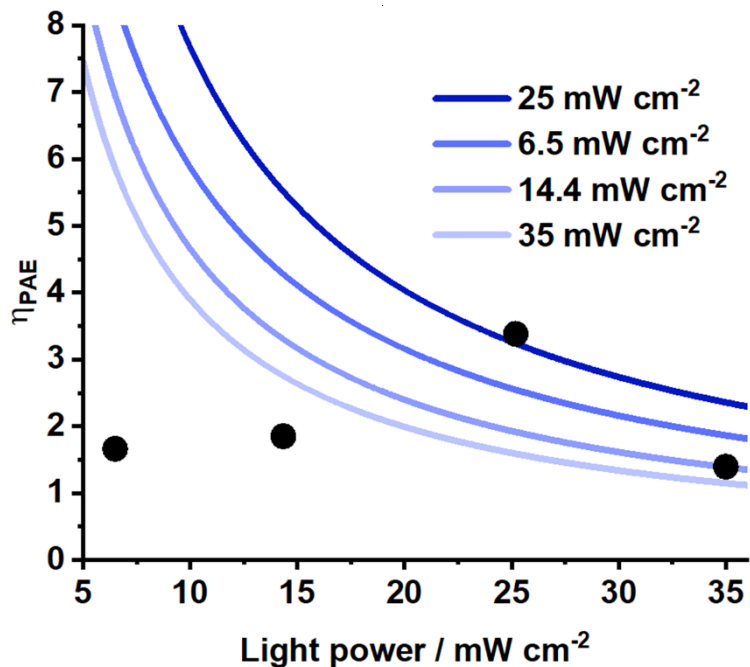


**Fig. S8.** Energy throughput conversion efficiency for photo-assisted electrolysis ( $\eta_{PAE}$ ) for configuration 1) and  $E_{cathode}$  at -2.15 V vs Ag/AgCl, KCl sat'd. Experimental data (black dots). Computed efficiency boundary line:  $E_{tot}$  from Fig. S6B, current density from Fig. S6D, and faradaic efficiency 90 %.

## 9. Table S1. Faradaic efficiency for configuration 1 (all products)

Light power / $mW\ cm^{-2}$	H <sub>2</sub> / %	CO / %	Formic acid / %	Total / %
6.5	7.6	0.5	85.0	93.1
14.4	4.0	0.4	86.8	91.2
25.2	4.9	0.3	93.6	98.8
35	8.1	0.5	78.9	87.5

## 10. Current without electric bias ( $E_{\text{tot}} = 0 \text{ V}$ )

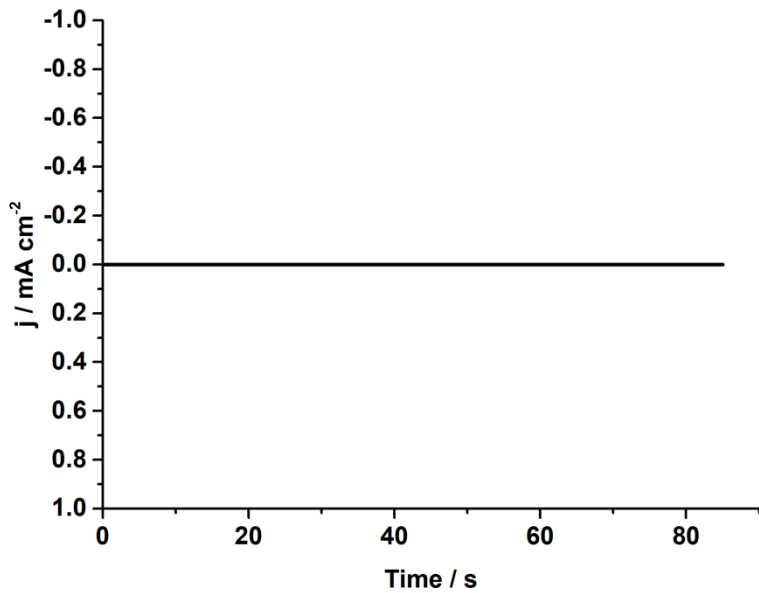


**Fig. S9.** Current measured without electric bias between TiO<sub>2</sub> NT and BDD electrodes in configuration 2 (i.e.,  $E_{\text{tot}} = 0 \text{ V}$ ). Light power 25.2 mW cm<sup>-2</sup>.

## 11. Potential and current for configuration 2

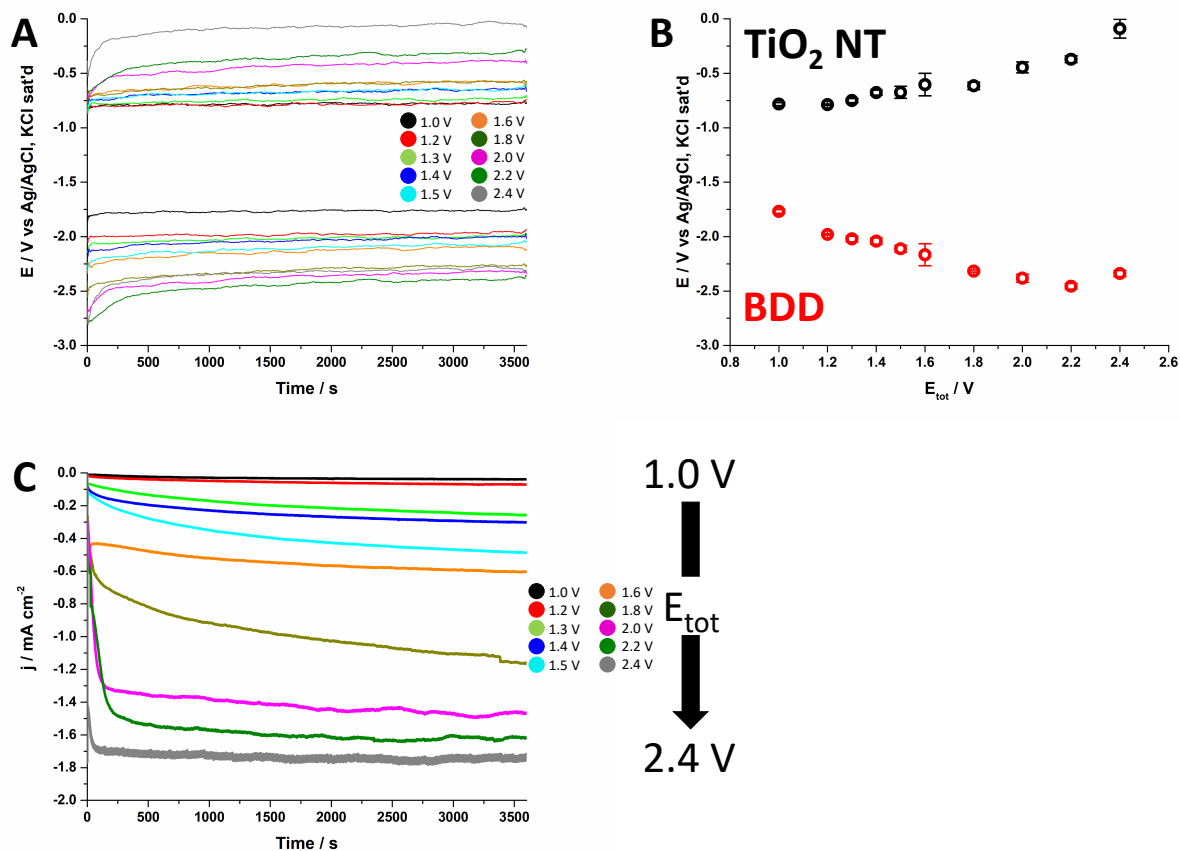


**Fig. S10.** A) Potential monitoring at  $\text{TiO}_2$  NT and BDD electrodes, and B) average potential as function of  $E_{tot}$ . C) current density variation with  $E_{tot}$ . Light intensity:  $25.2 \text{ mW cm}^{-2}$ . For clarity, A) and C) show only one measurement (average), while the measurements are repetition of 3 experiments (standard deviation in B).

## 12. Table S2. Faradaic efficiency for configuration 2 (all products)

$E_{tot} / V$	$\text{H}_2^{\text{a}} / \%$	$\text{CO} / \%$	$\text{Formic acid} / \%$	Total / %
1.0	$21.3 \pm 9.7$	$0.6 \pm 0.2$	$19.5 \pm 2.6$	$41.4 \pm 10$
1.2	$13.1 \pm 5.2$	$0.4 \pm 0.03$	$37.1 \pm 8.4$	$50.6 \pm 9.8$
1.3	$13.7 \pm 1.3$	$0.3 \pm 0.1$	$73.9 \pm 0.7$	$87.9 \pm 1.5$
1.4	$4.5 \pm 1.2$	$0.3 \pm 0.1$	$82.3 \pm 5.4$	$87.1 \pm 5.5$
1.5	$6.3 \pm 0.3$	$0.2 \pm 0.03$	$85.7 \pm 1.5$	$92.2 \pm 1.5$
1.6	$14.5 \pm 2.5$	$0.2 \pm 0.1$	$85.2 \pm 2.1$	$100.0 \pm 3.3$
1.8	$13.8 \pm 5.6$	$0.4 \pm 0.003$	$86.3 \pm 5.2$	$100.5 \pm 7.7$
2.0	$11.7 \pm 4.2$	$0.5 \pm 0.1$	$90.7 \pm 5.0$	$103.0 \pm 6.5$
2.2	$10.8 \pm 4.8$	$0.8 \pm 0.2$	$88.5 \pm 5.0$	$100.1 \pm 6.9$
2.4	$17.2 \pm 5.3$	$0.3 \pm 0.1$	$85.1 \pm 5.6$	$102.6 \pm 7.7$

<sup>a</sup> hydrogen might be underestimated because of leaking.

### 13. Control experiments for products confirmation

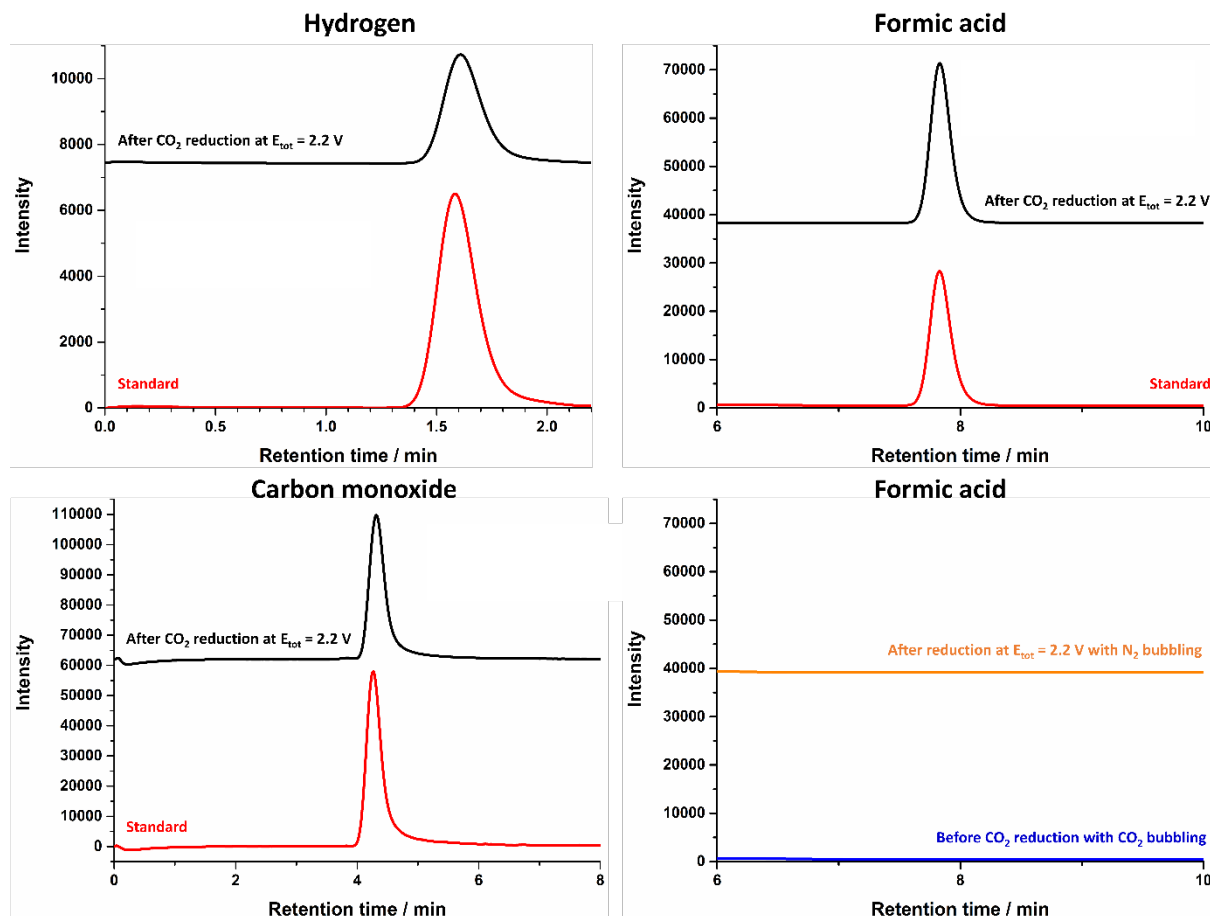


**Fig. S11.** HPLC chromatograms for different conditions to confirm formic acid produced by CO<sub>2</sub> reduction. Standard sample (red trace), and after CO<sub>2</sub> electrochemical reduction (black traces). For formic acid: after reduction at E<sub>tot</sub> 2.2 V with nitrogen bubbling (orange), and before reduction with CO<sub>2</sub> bubbling (blue).

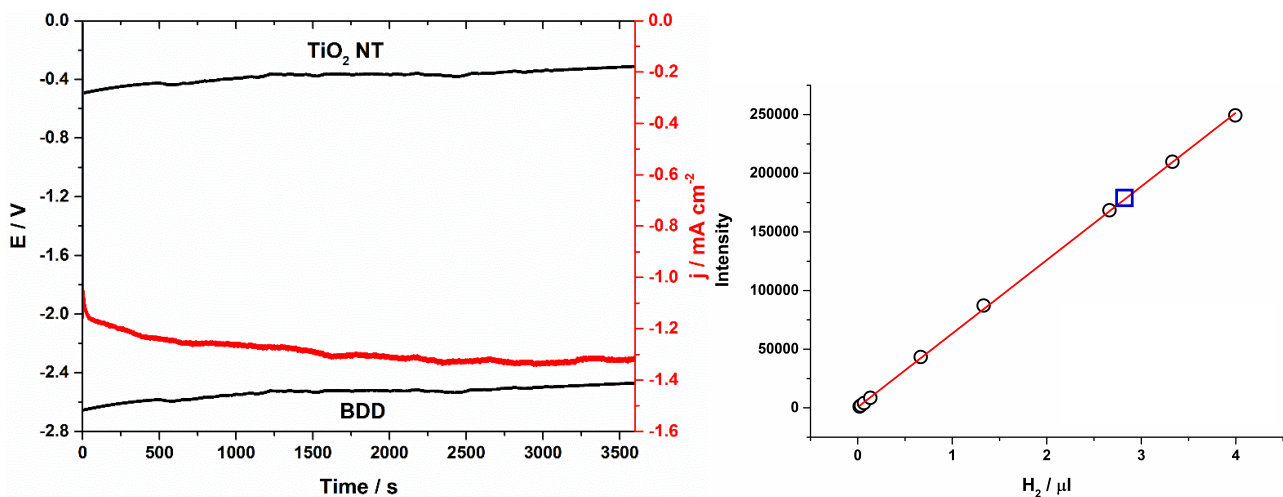


**Fig. S12.** Time dependence of potential at BDD and TiO<sub>2</sub> NT (black trace) and current (red trace) for reduction at E<sub>tot</sub> 2.2 V with nitrogen bubbling. Faradaic efficiency: H<sub>2</sub> (89.8%), CO (not detected), formic acid (not detected). Hydrogen calibration line and corresponding hydrogen signal (blue square) detected from GC analysis after the experiment.

## 14. Table S3. Efficiency comparison with other PEC systems

System	Anode	Cathode	FE	Current density / mA cm <sup>-2</sup>	$\eta_{PEC}$	$\eta_{ECE}$	Ref.
PEC	GaAs/ InGaP/TiO <sub>2</sub> / Ni	Pd/C-Ti mesh	94% (HCOOH)	8.5	10%	59.3%	2
PV + EC	IrO <sub>2</sub> Nanotubes	Cu-Ag Nanocoral	70% (CO/hydrocarbo ns/oxygenates)	9	4%	34%	3
PV + EC	SnO <sub>2</sub> /CuO	SnO <sub>2</sub> /CuO	86.6% (CO)	11.57	13.4%	47%	4
PEC	BiVO <sub>4</sub>	Cu	65% (HCOOH) / 0.75 V 80% (HCOH) / 0.9 V	0.10 0.36	0.3% (HCOOH) 0.7% (HCOH)	-	5
PV + EC	IrO <sub>x</sub>	Nanoporous Ag	93% (CO)	5.99	8.0%	44.6%	6
PV + EC	IrO <sub>2</sub>	OD-Au	80% to 90% (CO)	5.8	6.5%	48.5%	7
PEC	TiO <sub>2</sub> NT	BDD	86% (HCOOH)	1.7	5.6%	80%	This work

PEC: photoelectrochemical; PV: photovoltaic; EC: electrochemical;

## 15. Water oxidation potential at pH 14 (in 0.5 M KOH) vs Ag/AgCl (KCl sat'd)<sup>8,9</sup>

$$E_{\text{Ag/AgCl (KCl sat'd)}}^0 = E_{\text{NHE}}^0 - 0.197 - 0.059 \times \text{pH} = 1.229 - 0.197 - 0.826 = 0.206 \text{ V}$$

## 16. References

- 1 J. Xu, Y. Yokota, R. A. Wong, Y. Kim, and Y. Einaga, *J. Am. Chem. Soc.*, 2020, **142**, 2310-2316.
- 2 X. Zhou, R. Liu, K. Sun, Y. Chen, E. Verlage, S. A. Francis, N. S. Lewis and C. Xiang, *ACS Energy Lett.*, 2016, **1**, 764-770.
- 3 Gurudayal, J. Bullock, D. F. Sránkó, C. M. Towle, Y. Lum, M. Hettick, M. C. Scott, A. Javey and J. Ager, *Energy Environ. Sci.*, 2017, **10**, 2222-2230.
- 4 M. Schreier, F. Héroguel, L. Steier, S. Ahmad, J. S. Luterbacher, M. T. Mayer, J. Luo and M. Grätzel, *Nat. Energy*, 2017, **2**, 17087.

- 5 C. W. Kim, M. J. Kang, S. Ji and Y. S. Kang, *ACS Catalysis*, 2018, **8**, 968-974.
- 6 S. Y. Chae, S. Y. Lee, S. G. Han, H. Kim, J. Ko, S. Park, O.-S. Joo, D. Kim, Y. Kang, U. Lee, Y. J. Hwang and B. K. Min, *Sustainable Energy Fuels*, 2020, **4**, 199-212.
- 7 M. Schreier, L. Curvat, F. Giordano, L. Steier, A. Abate, S. M. Zakeeruddin, J. Luo, M. T. Mayer, M. Grätzel, *Nat. Commun.*, 2015, **6**, 7326.
- 8 T. J. Smith and K. J. Stevenson, Reference Electrodes, in C. G. Zoski Ed., *Handbook of Electrochemistry*, 2006, pp. 75.
- 9 G. Jerkiewicz, *ACS Catal.*, 2020, **10**, 8409-8417.